# *Tbata* modulates thymic stromal cell proliferation and thymus function

Francis A. Flomerfelt,[1] Nahed El Kassar,[1] Chandra Gurunathan,[1] Kevin S. Chua,[1] Stacy C. League,[1] Sabrina Schmitz,[1] Timothy R. Gershon,[2] Veena Kapoor,[1] Xiao-Yi Yan,[1] Ronald H. Schwartz,[3] and Ronald E. Gress[1]

[1]Experimental Transplantation Immunology Branch, National Cancer Institute, National Institutes of Health, Bethesda, MD 20892
[2]Department of Neurology, 6109E Neuroscience Research Building, University of North Carolina, Chapel Hill, NC 27599
[3]Laboratory of Cellular and Molecular Immunology, National Institute of Allergy and Infectious Disease, National Institutes of Health, Bethesda, MD 20892

**Niche availability provided by stromal cells is critical to thymus function. Thymi with diminished function contain fewer stromal cells, whereas thymi with robust function contain proliferating stromal cell populations. Here, we show that the thymus, brain, and testes–associated gene (*Tbata*; also known as SPATIAL) regulates thymic epithelial cell (TEC) proliferation and thymus size. *Tbata* is expressed in thymic stromal cells and interacts with the enzyme Uba3, thereby inhibiting the Nedd8 pathway and cell proliferation. Thymi from aged *Tbata*-deficient mice are larger and contain more dividing TECs than wild-type littermate controls. In addition, thymic reconstitution after bone marrow transplantation occurred more rapidly in *Rag2*$^{-/-}$*Tbata*$^{-/-}$ mice than in *Rag2*$^{-/-}$*Tbata*$^{+/+}$ littermate controls. These findings suggest that Tbata modulates thymus function by regulating stromal cell proliferation via the Nedd8 pathway.**

CORRESPONDENCE
Francis A. Flomerfelt:
flomerff@mail.nih.gov

Abbreviations used: AppBp1, amyloid protein precursor binding protein 1; BMT, BM transplantation; EGL, external germinal layer; mTEC, medullary TEC; Nedd8, neural precursor cell–expressed developmentally down-regulated 8; Tbata, thymus, brain, and testes–associated gene; TEC, thymic epithelial cell, Ttv, Tbata transcript variant.

Thymic stromal cell subsets form unique microenvironmental niches that support thymopoiesis and regulate thymus function as defined by the capacity to support T cell development and produce T cells (Anderson et al., 2000; Anderson and Jenkinson, 2001). Niche availability depends on the number and proliferative status of stromal cells. Therefore, conditions where stromal cells are maintained or increased by proliferation, such as in young animals, after castration, or in cyclinD1 transgenic mice, result in larger thymi, whereas reduced stromal cell proliferation, such as that observed in aged mice, results in smaller thymi (Klug et al., 2000; Gray et al., 2006; Williams et al., 2008). Although it is now accepted that stromal cell number plays a critical role in thymus function, not much is known regarding the molecular pathways involved in regulating their proliferation. To address this deficiency, we identified Tbata (thymus, brain, and testes–associated) based on its expression in thymic epithelial cells (TEC; Flomerfelt et al., 2000). Subsequent studies showed that Tbata is also expressed in fetal liver, lymph nodes, brain, and testes (Kim et al., 1998; Flomerfelt et al., 2000; Irla et al., 2003, 2007; Saade et al., 2007). Further work showed that Tbata physically associates with the kinesin motor protein KIF17 (Hirokawa and Takemura, 2004) in spermatids and in the brain (Irla et al., 2007; Saade et al., 2007). In studies aimed at determining the function of Tbata in the thymus, we created Tbata-deficient mice and identified another protein that interacts with Tbata. Here, we report our findings, which suggest that Tbata controls TEC proliferation and regulates thymic function.

The neural precursor cell–expressed developmentally down-regulated 8 (Nedd8) conjugation (neddylation) pathway is upstream of ubiquitin-mediated protein degradation and is an important regulator of cell proliferation (Rabut and Peter, 2008). Nedd8 is an ubiquitin-like molecule that is covalently ligated to cullin (Cul) family proteins (Hori et al., 1999; Xirodimas et al., 2004) by the sequential action of activating E1 and ligating E2 enzymes (Yeh et al., 2000). Uba3, the catalytic subunit of the



Supplemental material can be found at:
http://doi.org/10.1084/jem.20092759

The Rockefeller University Press $30.00
J. Exp. Med. Vol. 207 No. 11 2521-2532
www.jem.org/cgi/doi/10.1084/jem.20092759

activating enzyme complex, and amyloid protein precursor binding protein 1 (AppBp1) interact to form the Nedd8 E1 enzyme complex that initiates the Nedd8 pathway, whereas Ubc12 is the Nedd8 ligating E2 (Gong and Yeh, 1999). Neddylation activates Cul proteins, which are components of the Skp–Cul–F-box (SCF) protein complex targeting several cell cycle control proteins for degradation (Morimoto et al., 2000, 2003; Podust et al., 2000; Bloom et al., 2003) via the ubiquitin mediated proteasome pathway (Morimoto et al., 2000; Ohh et al., 2002).

Multiple lines of evidence support a role for the Nedd8 pathway in regulation of cell growth. First, Uba3-null preimplantation embryo cells fail to enter S-phase and die in utero (Tateishi et al., 2001), suggesting that cell cycle progression at this stage depends on neddylation. In addition, proteins that modulate the Nedd8 pathway affect the cell cycle. A dominant-negative Ubc12 mutant blocks cullin neddylation and cell cycle when overexpressed (Wada et al., 2000), whereas overexpression of Cul1 in c-myc–null MEF cells stimulates their growth (O'Hagan et al., 2000). Neddylation of Cul-3 regulates cyclin E degradation and S-phase entry in mammalian cells (Singer et al., 1999). In this article, we provide evidence that Tbata sequesters Uba3 and regulates thymus function by modulating stromal cell proliferation via interference with the Nedd8 pathway.

## RESULTS

### Tbata expression inversely correlates with TEC proliferation

While investigating stromal cell function in aged C57BL/6 thymi, we observed a 10-fold increase in steady-state mRNA levels of Tbata in C57BL/6 thymus from 4-mo-old mice versus 1-mo-old mice (Fig. 1 A). The increase in thymic Tbata expression at 4 mo of age correlates with the onset of decreased TEC proliferation and numbers observed in the C57BL/6 thymus during aging (Gray et al., 2006). In C57BL/6 mice aged 4–24 mo, the expression of Tbata remains high during a period when thymic stromal cells do not proliferate and their numbers steadily decline (Gray et al., 2006). Modest increases (two- to threefold) in Tbata expression were observed in cerebellum and testes during aging (Fig. S1, A and B). Although the pattern of Tbata expression during aging is similar in thymus, cerebellum, and testes, the magnitude of the age-dependent increase in the thymus is distinct. To extend our findings in the thymus, we examined DBA/2 mice that exhibit a more rapid and severe age-dependent decrease in thymus function compared with C57BL/6 mice (Hsu et al., 2003, 2005). Although Tbata levels in DBA/2 thymus were similar to C57BL/6 mice at 1 mo of age, we noted an 8–10-fold increase in Tbata mRNA levels in DBA/2 mice by 2 mo. By 3 mo, the level of Tbata mRNA had doubled again and remained high as the mice aged up to 9 mo (Fig. 1 A). Therefore, we observed high-level

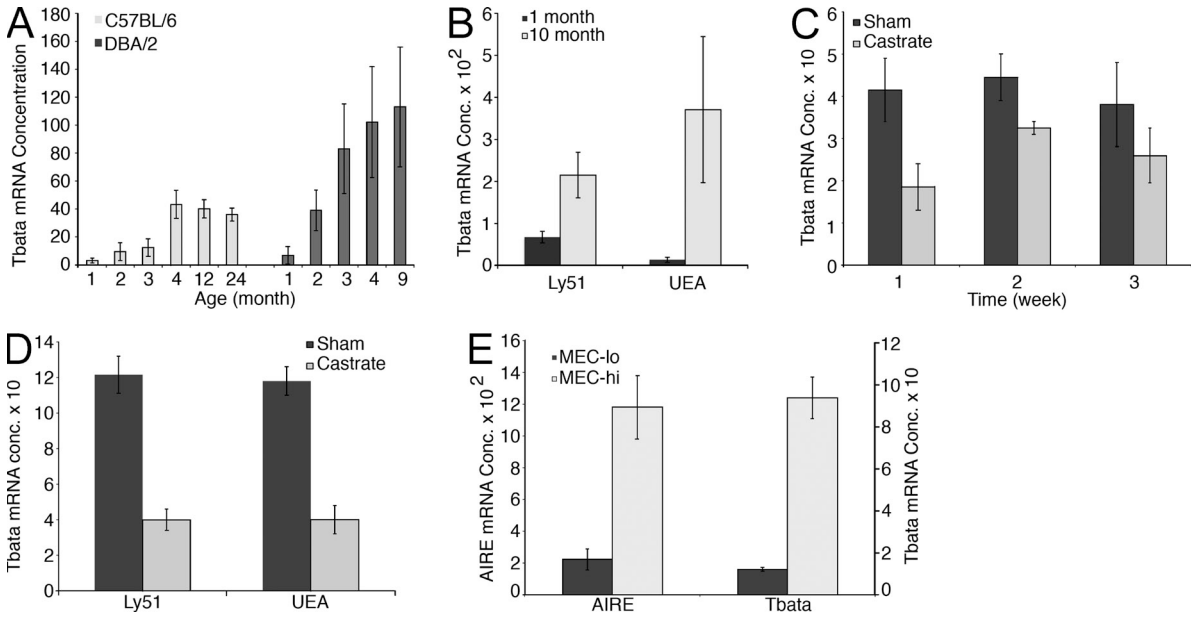


**Figure 1. High Tbata expression is associated with reduced thymus function.** (A) Tbata mRNA in thymi of aging C57BL/6 and DBA/2 mice was measured by real-time PCR. Values are expressed as the mean ± SD of independent experiments with 8–10 C57BL/6 mice and 5 DBA2 mice. (B) Amplified RNA from sorted CD45$^-$ and LY51$^+$ or UEA$^+$ thymic stromal cells from mice of indicated ages was used to perform quantitative real-time PCR. The relative Tbata expression level was calculated for each sample by normalizing to GAPDH. Data are derived from two independent experiments using cells sorted from 3–5 mice per group. (C) Mice ($n$ = 4) for each time point were castrated or sham-castrated for the indicated times and mRNA was prepared. Tbata expression was quantitated and normalized to GAPDH using real-time PCR. (D) Mice were castrated or sham-castrated and thymi were harvested after 1 wk. TECs were sorted from five pooled mice for each group. mRNA was isolated and Tbata expression was analyzed by real-time PCR and normalized using GAPDH. (E) UEA$^+$MHC class II$^{lo}$ (MEC$^{lo}$) or mature UEA$^+$ MHC class II$^{hi}$ (MEC$^{hi}$) mTECs were sorted. mRNA was isolated and AIRE (left), Ttv3, and Ttv5 levels were measured by real-time PCR and normalized using GAPDH expression. Data shown are the mean of four experiments using cells from two independent sorts. Error bars denote the SD.

Tbata expression during the period when thymus function is decreasing in these two strains of mice.

Given the changes in cellular composition of the thymus during aging, it was important to confirm that the increased Tbata expression observed was intrinsic to TEC. We examined Tbata levels in stromal cells sorted from 1- or 10-mo-old C57BL/6 mice (Fig. S1 C). Tbata RNA levels were increased about threefold in Ly51$^+$ cells and ~27-fold in UEA$^+$ cells sorted from the aged thymi (Fig. 1 B). Therefore, TEC isolated from aged thymi express higher levels of Tbata than those sorted from young thymi.

These data suggested that increased Tbata expression might play a role in decreasing thymus size. To explore whether Tbata expression might be dynamically regulated, we examined Tbata expression in response to a treatment that increases thymus size. An increase in thymus size coincident with an increase in the proportion and numbers of proliferating TEC occurs within 1 wk after castration in C57BL/6 mice (Gray et al., 2006; Williams et al., 2008). We measured Tbata expression in thymi from 4-mo-old castrates and sham-castrates over a 3-wk period after surgery. Within 1 wk, thymus weight increased ~2-3-fold (not depicted), whereas Tbata expression dropped by ~50% in castrated mice compared with sham-castrated controls (Fig. 1 C). Tbata expression continued to be lower in total thymi of castrated mice compared with controls over a 3-wk period. To confirm that the change in Tbata expression was TEC-specific, we sorted UEA$^+$ and Ly51$^+$ TEC from the thymi of castrated mice and sham-castrated mice one week after surgery. We observed a threefold decrease in both UEA$^+$ and Ly51$^+$ TEC (Fig. 1 D). The reduction of Tbata expression closely coincides with the onset of TEC proliferation and increased thymus size in C57BL/6 mice after castration that we, and others, have observed (Gray et al., 2006; Williams et al., 2008).

To explain these results, we hypothesized that high-level Tbata expression negatively regulates thymus function by regulating TEC proliferation. To further explore the connection between Tbata expression and TEC proliferation, we measured Tbata expression during medullary TEC (mTEC) development. During mTEC development, immature mTECs proliferate. After terminal differentiation, mature mTEC are MHC class II$^{hi}$, express AIRE, and exit the cell cycle (Gray et al., 2007). We sorted mTECs (CD45$^-$, Ly51$^-$) based on low (MEC$^{lo}$) or high (MEC$^{hi}$) MHC class II expression levels from 5-wk-old C57BL/6 mice (unpublished data). To evaluate our sort, we examined AIRE expression in both samples and found that expression was greater in the mature MEC$^{hi}$ subset, as expected (Fig. 1 E). Tbata was expressed in each subset but was increased by 5–10-fold in the MEC$^{hi}$ subset containing mature nonproliferating mTECs compared with the immature MEC$^{lo}$ subset (Fig. 1 E). Therefore, these data show that mTEC up-regulate Tbata expression as they mature and leave the cell cycle and provide further data supporting a relationship between Tbata expression and TEC proliferative status.

### Tbata inhibits cell growth

To directly test whether Tbata regulates the cell cycle, we performed growth assays after Tbata transfection. In these studies, we tested two Tbata isoforms, Tbata transcript variant 3 (Ttv3) and Tbata transcript variant 5 (Ttv5), created by alternative splice acceptor sites that differ by 34 aa (Flomerfelt et al., 2000). These two isoforms account for most Tbata expression in the thymus (unpublished data). In accord with our model, we observed that transient transfection of either Ttv3-EGFP or Ttv5-EGFP fusion proteins, but not control EGFP, blocked cell growth in transfected HEK 293T cells (Fig. 2 A). To examine division of Ttv3-EGFP–transfected cells we used DiI, a red fluorescent lipophylic dye that is equally portioned to each daughter during cell division (Huang et al., 1999). EGFP-transfected cells divided over a 4-d period, as indicated by a reduction in dye intensity (Fig. 2 B, top). In contrast, Ttv3-EGFP effectively blocked the majority of transfected cells from dividing (Fig. 2 B, bottom middle). The cell growth block was specific to cells expressing Ttv3-EGFP because untransfected cells (Fig. 2 B, bottom right) in the same culture divided normally. We also confirmed that Tbata mediates growth arrest in NIH3T3 cell lines that

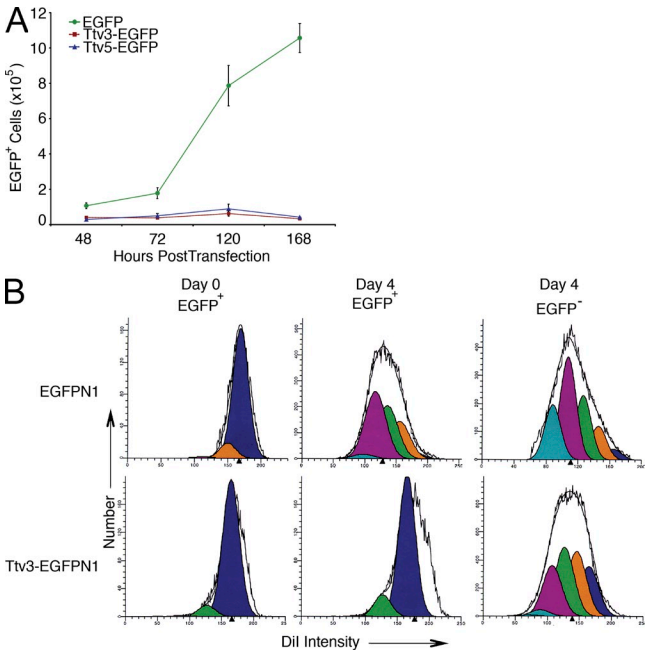


**Figure 2. Tbata mediates growth suppression of HEK 293 cells.** (A) Ttv3-EGFP (maroon square) or Ttv5-EGFP (blue triangle) or EGFP (green circle) fusion proteins were expressed in HEK293 cells, and growth was measured at indicated time points after transfection. The data in this experiment are representative of that obtained from >20 independent experiments. $n = 6$ for each time point. Error bars denote SD. (B) HEK 293 cells were transfected with EGFPN1 or Ttv3-EGFPN1. 1 d later, cells were labeled with DiI. Proliferation of $10^5$ EGFP$^+$ or EGFP$^-$ cells was determined using Modfit software to analyze flow cytometry data obtained 4 d after transfection. The different colored peaks represent generational divisions of the cell population calculated by the Modfit program. These data are representative of that obtained from four independent experiments.

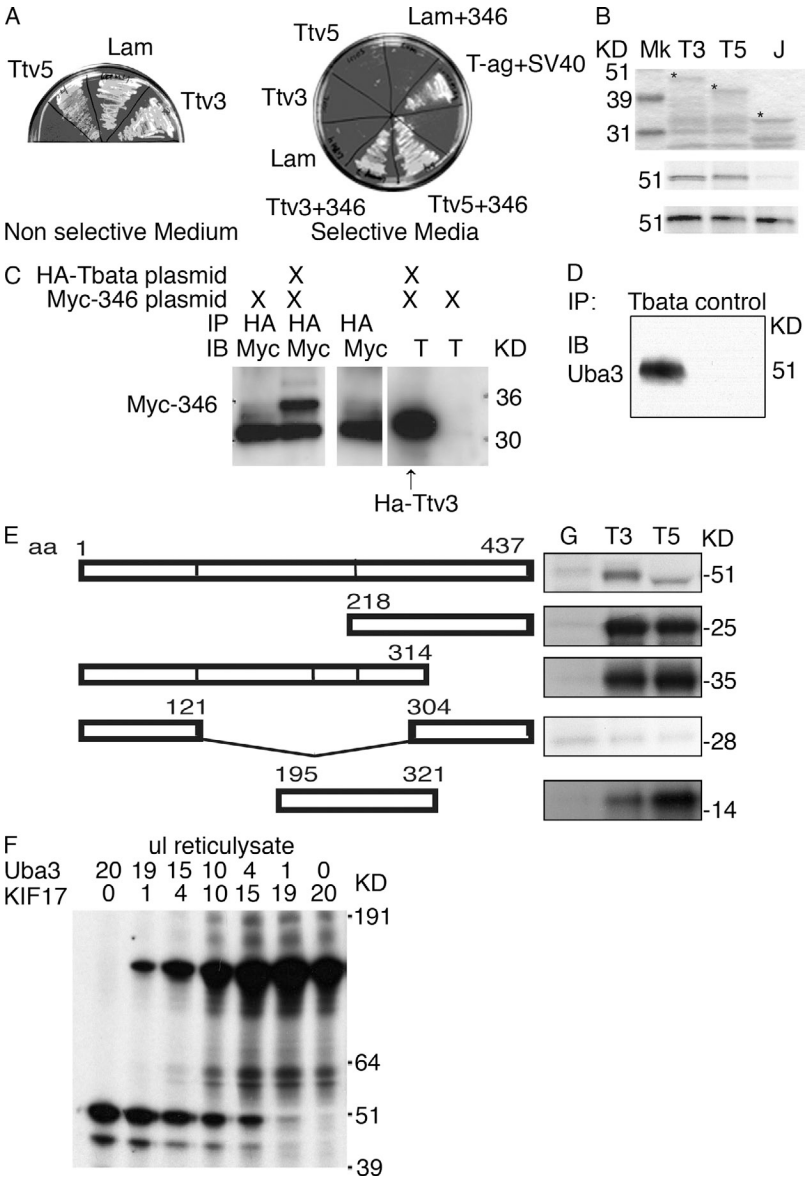


**Figure 3. Tbata specifically interacts with Uba3.** (A) Yeast strains expressing Tbata isoforms Ttv3 or Ttv5 or the irrelevant control Lamin C (Lam) were isolated after transfection of the indicated expression plasmid. The suitability of these strains to identify protein interaction with Tbata was tested by plating each of them on nonselective media or selective media lacking histidine and adenine. The capacity to interact with Uba3 was tested by transfecting the Uba3-346 expression plasmid into the tested yeast strains (creating strains Ttv3+346, Ttv5+346, and Lam+346) and plating on selective media. T-Ag+SV40 is a positive control yeast strain. These data are representative of that obtained from over five different independent experiments. (B) GST pulldown assays using radiolabeled Uba3 mixed with GST-Ttv3 (T3), GST-Ttv5 (T5), or GST-Jun (J). Top, stained gel with protein markers (Mk) to show input of GST fusion proteins (asterisks mark position of the full-length fusion proteins). Middle, autoradiograph of the same gel showing radiolabeled Uba3. Bottom, separate autoradiograph input of radiolabeled proteins used in the assay. The data in this experiment are representative of that obtained from >20 independent experiments done using different preparations of input proteins. (C) 293T cells were transfected with plasmids as indicated. Cell lysates were prepared and proteins were immunoprecipitated using a monoclonal anti-HA antibody and analyzed by Western blots with a monoclonal anti-Myc antibody (lanes 1–3) or a rabbit anti-Tbata antiserum (labeled T in lanes 4–5). The asterisk marks mouse IgG light chain in lanes 1–3. These data are similar to that obtained in three independent experiments. (D) Total thymus protein extracts were subjected to immunoprecipitation with an anti-Tbata rabbit antisera or a control rabbit IgG. Immunoprecipitated proteins were analyzed by Western blots using a commercially available goat anti-Uba3 (N17) and the Clean-Blot IP Detection kit that recognizes only native IgG. Similar results were obtained in a separate experiment using another thymus extract pooled from four mice. (E) Localization of the Uba3 domain that interacts with Tbata. GST pulldown assays shown on right, were done with GST (G), GST-Ttv3 (T3), or GST-Ttv5 (T5) using Uba3 and Uba3 deletion mutants shown diagrammatically. Similar results were obtained in three independent experiments. A slight amount of nonspecific binding to control GST-beads was sometimes observed and was equivalent to that observed with glutathione beads alone (not depicted). (F) Equal amounts of GST-Ttv3 were mixed with the indicated amounts of radiolabeled in vitro translated KIF17 and Uba3 proteins. This panel is representative of three independent experiments.

contain stably transfected mifepristone (mif)-inducible Ttv3-EGFP or EGFP expression cassettes (unpublished data). Using these inducible cell lines, we found that Tbata-dependent growth arrest is reversible because sorted Ttv3-EGFP– and Ttv5-EGFP–expressing cells resumed growth when placed in media lacking mif (unpublished data). Therefore, these data show that Tbata expression results in growth arrest.

### Tbata interacts with Uba3

To gain insight into Tbata function in regulating cell proliferation at a molecular level, we used the yeast 2-hybrid assay to screen an 18-d-old mouse embryo cDNA library for Tbata-interacting proteins and identified a cDNA (designated Uba3-346) encoding 235 aa of the carboxyl terminus of Uba3. To confirm the interaction, the Uba3-346 prey plasmid was transformed into yeast strains expressing Ttv3, Ttv5, or Lamin C (Lam). Strains expressing a Tbata isoform and Uba3-346 grew on selective media, whereas those expressing the LaminC-Uba3-346 combination did not (Fig. 3 A), providing genetic evidence that Tbata and Uba3 interact.

We used GST-pulldown and coimmunoprecipitation assays to confirm the interaction. Full-length radiolabeled Uba3 interacted with GST-Ttv3 and GST-Ttv5, but not with GST–Jun fusion proteins (Fig. 3 B, top). Tbata and Uba3 also interact when transfected and expressed in 293T cells (Fig. 3 C). In this experiment, Myc-Uba3-346 was immunoprecipitated

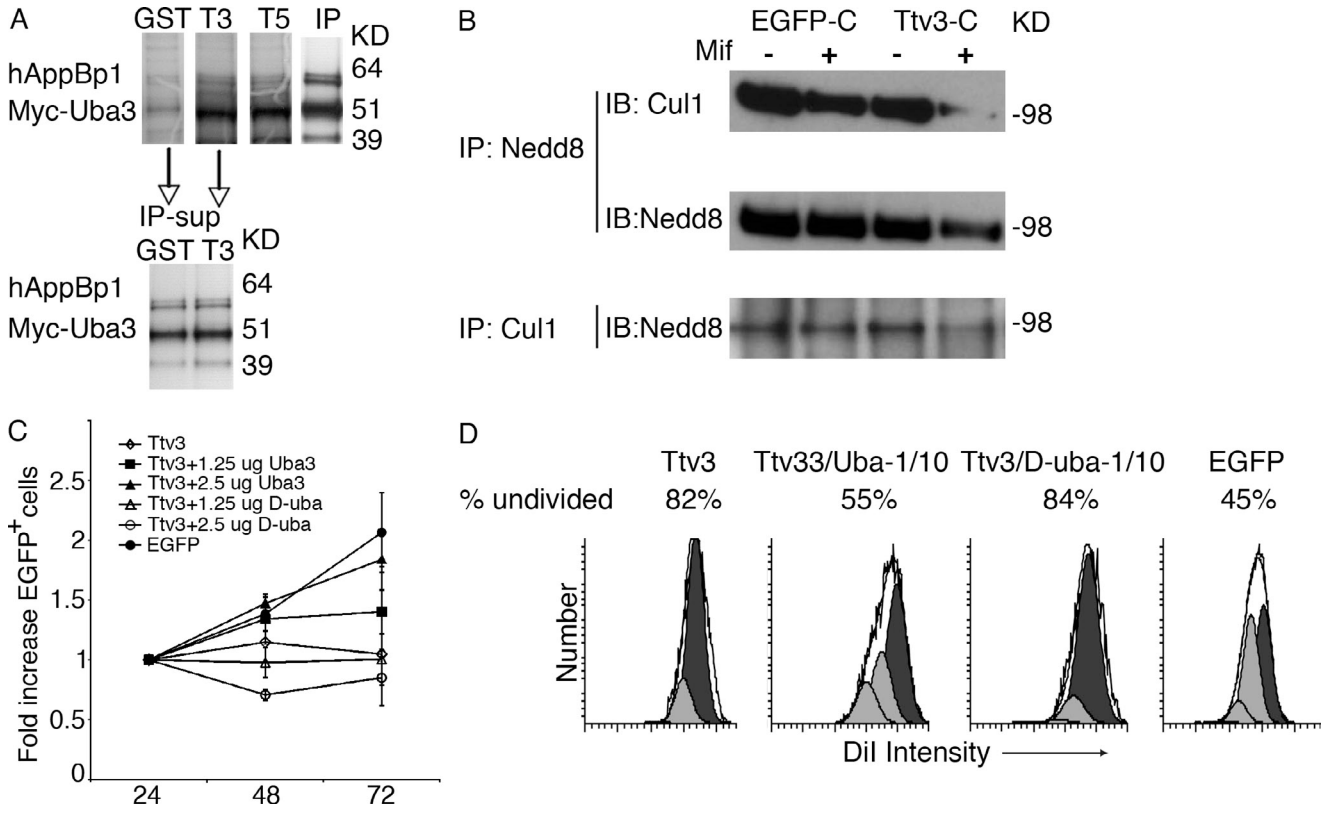


**Figure 4. Tbata interaction with Uba3 blocks formation of the Nedd8 E1 and inhibits cell division.** (A) GST pulldown assays were done with GST, GST-Ttv3 (T3), and GST-Ttv5 (T5) beads added to equal amounts of radiolabeled Myc-Uba3 and human AppBp1. Anti-Myc immunoprecipitations were used as a positive control using either Myc-Uba3 mixed with AppBp1 alone (IP) or from the supernatants of GST-Ttv3 (IP T3 sup) or GST (IP GST sup) pulldown assays (bottom). The asterisk shows the position of a protein differing by 8.7 kD produced during in vitro translation of Uba3 cDNA caused by usage of different ATG codons (Gong and Yeh, 1999). (B) The mif-inducible cell lines, EGFP-C and Ttv3-C were treated with mif ($10^{-8}$ M) to express EGFP (EGFP-C+mif) and Ttv3-EGFP fusion protein (Ttv3-C+mif), respectively. The whole-cell lysates were immunoprecipitated and immunoblotted as indicated. The blot was stripped and reprobed with rabbit nedd8 antibody (middle). (C) HEK 293 cells were transfected with 0.25 mg Ttv3-EGFP and different amounts of either Uba3 or D-uba3 DNA (◇, 0 mg; ■, 1.25 mg Uba3; △, 1.25 mg D-uba3; ▲, 2.5 mg Uba3; ○, 2.5 mg D-uba3). Control (◆) was transfected with 0.25 mg EGFP. Absolute cell numbers were measured at indicated times after transfection. Data shown is representative of five independent experiments done in triplicate. (D) HEK 293 cells were transfected with indicated plasmids alone on in a combination at 1:10 ratio. T3, Ttv3-EGFP; Uba, Uba3; D-Uba, D-Uba3.

by anti-HA antibody in samples that contained HA-Tbata (Fig. 3 C, lane 2), but not in untransfected cells (Fig. 3 C, lane 3) or in cells transfected with Uba3-346 alone (Fig. 3 C, lane 1). In addition, Tbata-Uba3 binding was observed in protein extracts obtained from thymus when immunoprecipitated using an anti-Tbata rabbit antisera (Fig. 3 D). To map the interaction site, a series of Uba3 deletion mutants was produced and tested for specific interaction with the Tbata isoforms Ttv3 and Ttv5 (Fig. 3 E). GST-Ttv3 and GST-Ttv5, but not GST, interacted with Uba3 mutants that lack the amino and carboxyl terminus of the protein. Removal of the central portion of Uba3 abolishes the interaction, whereas amino acids 195–321 of Uba3 retain the ability to interact with Tbata.

Because Tbata has been previously reported to also physically associate with KIF17 (Irla et al., 2007; Saade et al., 2007), we examined whether Tbata preferentially binds with either protein. The results of a series of Tbata binding assays performed with differing amounts of either radiolabeled protein showed that Tbata can bind both Uba3 and KIF17 simultaneously. Tbata interacts with both KIF17 and Uba3 even when these proteins were present at a 1:19 ratio (Fig. 3 F). Therefore, these proteins do not appear to compete for binding to Tbata in the conditions used in these in vitro binding assays.

### Tbata blocks Nedd8 E1 assembly

Given the evidence that Uba3 plays a central role in the Nedd8 pathway, we examined the effect of the Tbata–Uba3 interaction on the assembly of the Nedd8 E1. GST, Ttv3-GST, or Ttv5-GST was combined with radiolabeled Uba3 (Myc-tagged) and AppBp1. Immunoprecipitation of Myc-tagged Uba3 efficiently coprecipitated AppBp1 as expected (Fig. 4 A, IP lane). In contrast, when Ttv3-GST or Ttv5-GST interacted with Uba3, AppBp1 was not appreciably coprecipitated using glutathione–Sepharose (Fig. 4 A, lanes Ttv3 and Ttv5). The slight amount of AppBp1 observed may be caused by the ability of Uba3 to form dimers (Walden et al., 2003).

The neddylation of Cullin1 was examined in NIH3T3 cell lines that contain mifepristone (mif)-inducible Ttv3-EGFP or EGFP expression cassettes. A Nedd8 antibody was used to immunoprecipitate protein from extracts obtained from EGFP or Ttv3-EGFP–expressing cells. The immunoprecipitated proteins were analyzed by immunoblotting using an anti-Cullin1 antibody. There was a significant reduction in the level of neddylated Cullin1 in mif-treated cells expressing Ttv3-EGFP compared with mif-treated cells expressing EGFP (Fig. 4 B). Therefore, Tbata binding to Uba3 interferes with the Uba3–AppBp1 interaction and greatly reduces the level of neddylated Cullin1.

Given the role of the Nedd8 pathway in cell cycle control, it seemed likely that Tbata-mediated growth arrest was caused by its ability to bind Uba3 and block its function. To test this prediction, we examined whether overexpression of Uba3 would prevent Tbata-dependent growth arrest in cell lines expressing transfected Tbata. Increasing amounts of either Uba3 or control d-uba3 (Fig. 3 E, deletion 121–304) expression plasmids were cotransfected in HEK 293 cells with a fixed amount of Ttv3-EGFP. Ttv3-EGFP–transfected cells grew more over a 3-d period when Uba3 was overexpressed (Fig. 4 C). The growth was dose dependent (compare 1.25 µg to 2.5 µg Uba3 transfections). Tbata-mediated growth arrest was unaffected in control cells overexpressing D-uba3 that does not bind Tbata. Finally, labeling with DiI confirmed that coexpression of Tbata-EGFP and Uba3 partially restored cell division, whereas cotransfection with D-uba3 did not (Fig. 4 D). The Ttv3-EGFP–dependent growth inhibition was also confirmed by experiments using both BrdU and DNA content analysis (unpublished data). Given that Tbata can simultaneously bind both Uba3 and the kinesin motor protein KIF17, we wanted to determine whether KIF17 coexpression affects Tbata-dependent growth suppression. We determined that KIF17 is not expressed in the thymus, in purified TEC, or in our inducible NIH3T3 cells as measured by RT-PCR (Fig. S1 d). Tbata mediates potent growth suppression in HEK 293 cells (Fig. 2 and Fig. 4) that express KIF17 mRNA (Fig. S1 d). Tbata-mediated growth suppression in HEK 293 cells is reversed by Uba3 overexpression (Fig. 4 D). These data indicate that KIF17 does not affect the ability of Tbata to block the Nedd8 pathway or affect Tbata-mediated growth inhibition in HEK 293T cells. Tbata-mediated growth inhibition was unaffected by overexpression of transiently transfected KIF17 fused to mCherry in our mifepristone-inducible Tbata NIH3T3 cell line Ttv3-C (Fig. S1 e). Although Tbata interacts with KIF17 in other organs (Irla et al., 2007; Saade et al., 2007), it is likely that KIF17 does not have a role in TEC function and does not affect Tbata-mediated growth suppression in the experimental models used in this study. Collectively, these data suggest that Tbata inhibits cell division by blocking the Nedd8 pathway.

### Tbata influences thymus function

The in vitro data concerning the molecular pathways by which Tbata inhibited the Nedd8 pathway and cell proliferation supported the previously generated data linking Tbata expression and thymus function. To more directly examine the in vivo role of Tbata on thymus function, a *Tbata* KO mouse model was developed (Fig. S2, A–D). *Tbata*$^{-/-}$ mice were viable, and both females and males were normally fertile throughout life. Because Tbata is also expressed in the testis and cerebellum, we also examined the structure and proliferative status of these organs in *Tbata*$^{-/-}$ mice. Male *Tbata*$^{-/-}$ mice exhibited normal testes morphology (Fig. S2 E) and function. Furthermore, there were no obvious neurological problems (unpublished data) or any obvious defects in gross brain anatomy. We did, however, note abundant, abnormal nests of retained external germinal layer (EGL) in the cerebellum. The EGL is normally depopulated by postnatal day 18 in WT mice as progenitors migrate to the internal granule cell layer and differentiate (Hatten and Heintz, 1995). In *Tbata*$^{-/-}$ mice, clumps of EGL cells remained evident at 1 mo of age and persisted in aged mice (Fig. S2 F). Therefore, the Tbata deficiency appears to have a minimal impact on testes function but did effect some changes in cerebellum development.

In contrast, we did observe changes in the thymus of *Tbata*$^{-/-}$ mice. In 1–2-mo-old *Tbata*$^{-/-}$ mice, there were no significant differences in the thymus between *Tbata*$^{-/-}$ and WT littermates (Fig. 5 A and not depicted). However, in 5–9-mo-old *Tbata*$^{-/-}$ mice, the thymus contained about twice as many thymocytes as WT littermates (Fig. 5 A). In 1-yr-old mice there was a fourfold greater number of thymocytes (Fig. 5 A) and about twice as many stromal cells (Fig. 5 B) in *Tbata*$^{-/-}$ mice compared with WT littermates. The rate of age-dependent thymus size decrease was slowed in the *Tbata*$^{-/-}$ and thymus size was consistently greater in aged *Tbata*$^{-/-}$ mice compared with WT littermates (Fig. 5 A). In spite of the differences noted in thymic cellularity, there were no differences in the numbers or ratios of either their B or T cells or in the CD4/CD8 ratios in spleen or lymph nodes (unpublished data) when *Tbata*$^{-/-}$ mice were compared with WT controls. We did observe a 1.5-fold increase in CD44$^{lo}$, CD62L$^{+}$ splenic T cells in aged mice consistent with their larger thymus (unpublished data). Thus, the Tbata deficiency resulted in a larger thymus in aged mice.

### Normal T cell development and function in *Tbata*$^{-/-}$ mice

We next addressed whether T cell development was affected in aged *Tbata*$^{-/-}$ mice. The absolute numbers of all thymocyte subsets were consistently greater in aged *Tbata*$^{-/-}$ mice compared with 9–12-mo-old WT mice (Fig. 5, C–E). There were 4–5 times more CD4 and CD8 double-negative DN cells in *Tbata*$^{-/-}$ mice than in WT littermates (Fig. 5, C and E). CD4 and CD8 double-positive, CD4, and CD8 populations were increased by three- to fourfold in the *Tbata*$^{-/-}$ mice (Fig. 5, D and E). We noted a slight increase in the percentage of DN cells in the *Tbata*$^{-/-}$ thymus, whereas the percentages of cells in the other subsets were similar to WT controls (Fig. 5, C–E). No defects in positive or negative selection were observed when *Tbata*$^{-/-}$ were crossed to the HY or 5CC7 TCR transgenics, although thymus size was larger

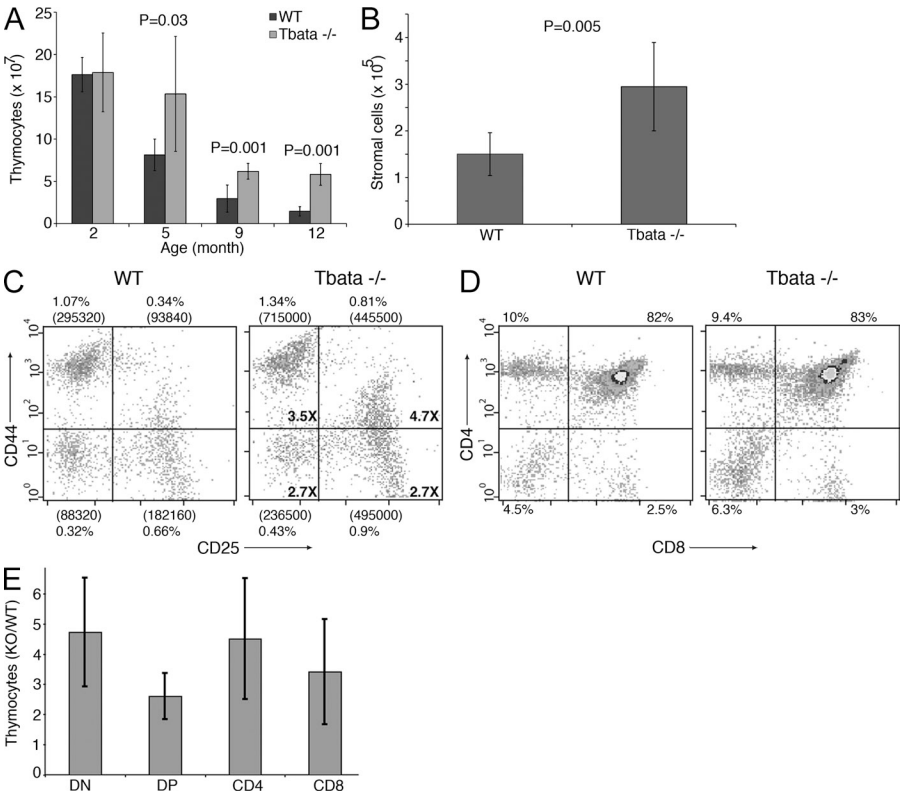


**Figure 5. Greater numbers of thymocytes develop normally in aged *Tbata*$^{-/-}$ mice.** (A) The mean number of thymocytes from WT or homozygote *Tbata*$^{-/-}$ thymi was calculated based on FACS analysis using CD45 or CD90 staining. Each group included 5 mice, except for the 12-mo time point where 9 WT and 10 KO mice were analyzed. (B) Stromal cells in 12–14-mo-old WT and *Tbata*$^{-/-}$ mice were calculated based on the percent of CD45$^{-}$HSA$^{-}$ cells in thymus suspensions. $n = 8$ mice/genotype (C). Expression pattern of CD44 and CD25 gated on Lin$^{-}$ (CD4, CD8, CD3, B220, and CD11b) cells from 9-mo-old mice. The percentages of total thymocytes for each quadrant and total cell number of each compartment are shown (in parenthesis). Numbers shown in quadrants of KO plot are fold increase in cell number compared with WT littermates. (D) Expression pattern of CD4 and CD8 on thymocytes from 9-mo-old mice. The percentages of total thymocytes in each quadrant are shown. (E) The mean of the ratios of KO/WT thymocyte numbers in each developmental stage in 10–12-mo-old mice was calculated after FACS analysis. WT (WT $n = 5$) and *Tbata*$^{-/-}$ (KO $n = 6$). Error bars in bar graphs denote the SD.

compared with *Tbata*$^{+}$ control mice (unpublished data). We also observed normal thymic architecture in 5-mo-old TKO, using anti-keratin 8 (red) to reveal cortical TEC and anti-keratin 5 (green) to visualize medullary TEC in frozen sections (Fig. S3 A). Mature T cells from *Tbata*$^{-/-}$ lymph nodes proliferated normally to immunization with a defined antigen (Fig. S3 B). Therefore, while aged *Tbata*$^{-/-}$ mice have larger thymi, the Tbata deficiency did not disrupt normal thymocyte development, thymus morphology, or T cell function.

### Rapid thymus reconstitution in *Tbata*$^{-/-}$*Rag2*$^{-/-}$ mice

To further examine the effect of Tbata-deficiency on thymus function, *Tbata*$^{-/-}$ mice were crossed to *Rag2*$^{-/-}$ mice (Shinkai et al., 1992) to create Tbata$^{-/-}$P$\alpha\gamma$2$^{-/-}$ double KO mice. The proportions of DN1-3 were normal in thymi from *Tbata*$^{-/-}$*Rag2*$^{-/-}$ mice and, as expected, thymocyte development was arrested at the DN3 stage (Fig. 6 A). We observed an increase in total thymocyte numbers in *Tbata*$^{-/-}$*Rag2*$^{-/-}$ mice 8 wk after birth (not depicted) and by 3 mo the thymi of *Tbata*$^{-/-}$*Rag2*$^{-/-}$ mice contained ~3-4 times more thymocytes (Fig. 6 B). There were about twice as many early thymocyte progenitors (ETPs; CD44$^{hi}$, c-kit$^{hi}$, CD25$^{-}$, and Lin$^{-}$) in *Tbata*$^{-/-}$*Rag2*$^{-/-}$ thymi (Fig. 6 C) than in *Rag2*$^{-/-}$ mice. Therefore, the Tbata deficiency causes an increase in thymocyte numbers in *Rag2*$^{-/-}$ mice, as well as in aged mice.

To confirm that the phenotype observed in *Tbata*$^{-/-}$ thymus was caused by alterations in stromal cells, we examined thymus recovery after BM transplantation (BMT) in the *Tbata*$^{-/-}$*Rag2*$^{-/-}$ versus control littermates. T cell depleted Ly5.1$^{+}$ BM cells from WT mice were injected into adult *Tbata*$^{-/-}$*Rag2*$^{-/-}$ mice. Age-matched littermates (*Tbata*$^{+/+}$, *Rag2*$^{-/-}$) were used as controls. Ly5.1$^{+}$, B220$^{+}$ cell numbers were used to show that the engraftment of donor cells in different mice was comparable (Fig. S4). Interestingly, thymic reconstitution in the *Tbata*$^{-/-}$*Rag2*$^{-/-}$ thymus occurred faster than was observed in a *Rag2*$^{-/-}$ mouse (Fig. 6 F). Within 3 wk, all thymocyte developmental stages, derived from donor cells were present in transplanted *Tbata*$^{-/-}$*Rag2*$^{-/-}$ mice (Fig. 6, D and E). In *Rag2*$^{-/-}$ mice, donor cells were present but a comparable state of reconstitution was not reached for another 10–14 d (unpublished data). At 5 wk after transplant, both the *Tbata*$^{-/-}$*Rag2*$^{-/-}$ and the *Rag2*$^{-/-}$ mice had full reconstitution of all thymic subsets, but the total number of donor thymocytes in the *Tbata*$^{-/-}$*Rag2*$^{-/-}$ was about sevenfold greater than in the *Rag2*$^{-/-}$ mice (Fig. 6 F). By 9 wk after BMT; thymic reconstitution in both *Rag2*$^{-/-}$ mice and *Tbata*$^{-/-}$*Rag2*$^{-/-}$ mice was similar (Fig. 6 F). The rapid thymic reconstitution in *Tbata*$^{-/-}$*Rag2*$^{-/-}$ mice was accompanied by a more rapid repopulation of the periphery by donor T cells (Fig. 6 G). Therefore, *Tbata*$^{-/-}$*Rag2*$^{-/-}$ mice have improved thymus reconstitution relative to control mice as measured by reconstitution of thymocyte subpopulations and production of mature T cells providing additional evidence that Tbata affects thymus function.

### TEC proliferation in *Tbata*$^{-/-}$ mice

We hypothesized that the increase in thymus size observed in aged *Tbata*$^{-/-}$ mice was caused by enhanced TEC proliferation.

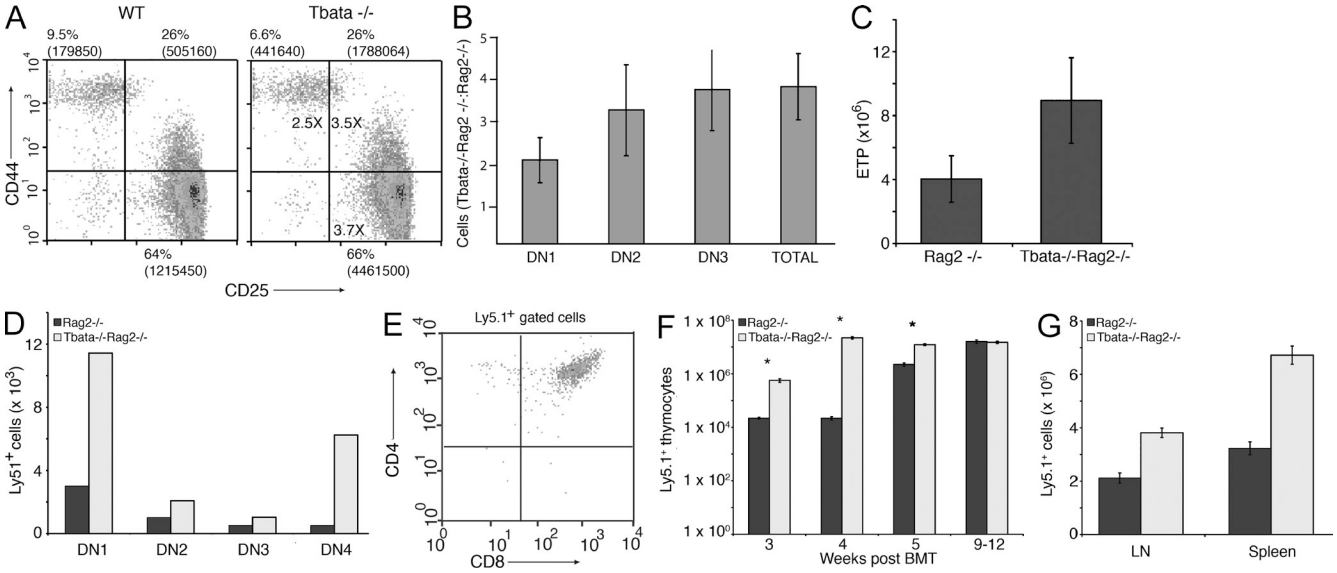


**Figure 6. Tbata$^{-/-}$Rag2$^{-/-}$ mice have increased thymocytes and enhanced thymic reconstitution dependent on stromal cells after BM transplant.** (A) A representative CD44 versus CD25 FACS profile of thymocytes from a *Rag2*$^{-/-}$ or a *Tbata*$^{-/-}$*Rag2*$^{-/-}$ mouse is shown. Percentage total for each quadrant is shown with total cell number in parenthesis. Numbers shown in quadrants of the *Tbata*$^{-/-}$*Rag2*$^{-/-}$ plots are the fold increase in cell number compared with the control *Rag2*$^{-/-}$ littermates. Similar results were obtained in at least four independent experiments. (B) Mean ratios of thymocyte numbers were calculated as in Fig. 5 from *Tbata*$^{-/-}$ *Rag2*$^{-/-}$ DKO; $n = 6$) and *Rag2*$^{-/-}$ (KO; $n = 5$) littermates. (C) Mean ETP (Lin$^-$, CD25$^-$, CD44$^+$, and CD117$^+$) numbers for *Tbata*$^{-/-}$ *Rag2*$^{-/-}$ or *Rag2*$^{-/-}$ mice are shown. All mice were 3 mo old (*Tbata*$^{-/-}$*Rag2*$^{-/-}$, $n = 6$, *Rag2*$^{-/-}$, $n = 6$). Panels D and E are data obtained from single mice representative of the results we obtained from three independent experiments with 7 *Tbata*$^{-/-}$*Rag2*$^{-/-}$ and 6 *Rag2*$^{-/-}$ mice at the 3-wk time point. (D and E) *Rag2*$^{-/-}$*Tbata*$^{+/+}$ and *Rag2*$^{-/-}$*Tbata*$^{-/-}$ mice were injected with Ly5.1$^+$ BM, and Ly5.1$^+$ thymocytes were analyzed 3 wk later. (F) Numbers of Ly5.1$^+$ thymocytes. Four independent experiments were quantitated over time after BMT. *, $P < 0.001$. 7 *Tbata*$^{-/-}$*Rag2*$^{-/-}$, 6 *Rag2*$^{-/-}$ (3 wk); 3 *Tbata*$^{-/-}$*Rag2*$^{-/-}$, 3 *Rag2*$^{-/-}$ (4 wk); 3 *Tbata*$^{-/-}$*Rag2*$^{-/-}$, 3 *Rag2*$^{-/-}$ (5 wk); 4 *Tbata*$^{-/-}$*Rag2*$^{-/-}$, 4 *Rag2*$^{-/-}$ (9–12 wk). (G) Numbers of Ly5.1$^+$ T cells in the spleen and LN 5 wk after BM transplantation. Data shown is the mean of three *Tbata*$^{-/-}$*Rag2*$^{-/-}$ and three control *Rag2*$^{-/-}$ littermates. Similar results were obtained from two additional independent experiments. Error bars in bar graphs of all panels denote the SD.

Therefore, we examined TEC proliferation in 6–9-mo-old mice because this is the earliest period when differences in thymus size between WT and *Tbata*$^{-/-}$ mice are evident. We analyzed mTEC (UEA$^+$, ClassII$^+$) and cTEC (Ly51$^+$, ClassII$^+$) from 6–9-mo-old WT or *Tbata*$^{-/-}$ mice using flow cytometry. The percentages of TEC subsets in *Tbata*$^{-/-}$ and WT mice at these ages were similar, except for a twofold increase in the percentage of MEC-lo cells as a fraction of total TEC ($P = 0.009$; unpublished data). There were significantly more TECs in the *Tbata*$^{-/-}$ thymi ($P = 0.02$) compared with WT littermates, and both cTEC and mTEC numbers were increased (Fig. 7 A). However, the cTEC/mTEC ratios (WT, 2.06; *Tbata*$^{-/-}$, 2.07; unpublished data) were the same in both sets of mice. Using Ki67 staining, we observed a significant increase in the numbers of proliferating UEA$^+$ mTEC in *Tbata*$^{-/-}$ mice both in MEC$^{lo}$ and MEC$^{hi}$ fractions, whereas numbers of proliferating cTECs were modestly increased (Fig. 7 B). Similar data were obtained in other experiments using BrdU to assess TEC proliferation (unpublished data). Therefore, Tbata appears to play a role in regulating TEC proliferation in this setting.

## DISCUSSION

T cell development depends on a complex interplay between BM-derived lymphoid progenitor cells and resident stromal cells (Anderson and Jenkinson, 2001). Recent findings highlight the relationship between stromal cell proliferation and numbers with thymus function as observed in a K5-CyclinD1 transgenic, in Nude-Wt chimeras, or in aged thymus (Robles et al., 1996; Klug et al., 2000; Gray et al., 2006; Jenkinson et al., 2008). Therefore, an understanding of the mechanisms that regulate stromal cell numbers might identify control

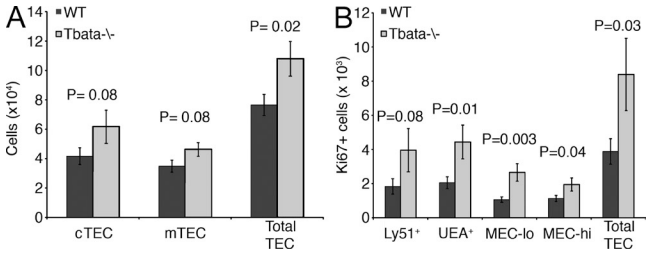


**Figure 7. Increased numbers of TECs proliferate in *Tbata*$^{-/-}$ mice.** (A) Numbers of TECs were measured in 6–9-mo-old *Tbata*$^{-/-}$ mice and WT age-matched littermates. Mean values were calculated after determining percentages of the indicated subsets by FACS analysis of Ly51$^+$ClassII$^+$ to identify cTEC and UEA$^+$ClassII$^+$ to identify mTEC (*Tbata*$^{-/-}$, $n = 10$; WT, $n = 17$). (B) Enriched thymic stromal cell suspensions were stained with CD45, MHC ClassII, UEA, and Ly51. The numbers of proliferating cells were calculated after determining the percentages of Ki67$^+$ cells in the indicated subsets by FACS analysis (*Tbata*$^{-/-}$, $n = 10$; WT, $n = 17$). Error bars shown in all panels denote the SD.

points of thymus function and provide strategies to improve T cell production in immunodeficient patients. To increase our basic understanding of stromal cell function in the thymus, we cloned Tbata (Kim et al., 1998). Initially, we reported that Tbata expression was restricted to the subcapsule of adult mice (Flomerfelt et al., 2000). Using more sensitive techniques, however, we now report that Tbata is also expressed in cortical and medullary TECs in accord with the findings of others (Flomerfelt et al., 2000; Saade et al., 2007). In this study, we provide strong evidence that Tbata exerts a reversible negative regulatory effect on cell proliferation and thymus function.

Our data show that changes in the level of Tbata expression in the thymus correlates with the state of TEC proliferation, as we demonstrated in four different situations. First, Tbata levels are lowest in young thymus when TEC proliferation is robust (Gray et al., 2006) and are increased 10-fold in C57BL/6 mice 4 mo of age or older, coincident with reduced proliferation and a reduction of TEC numbers over time. Second, Tbata levels vary in mouse strains with different rates of age-dependent loss of thymus function. DBA/2 mice rapidly lose thymus function (Hsu et al., 2003) and exhibit an earlier and greater increase in Tbata expression compared with C57BL/6 mice. In accord with our phenotypic data, *Tbata*$^{-/-}$ resides on chromosome 10 in a region identified as a genetic locus involved in the early reduction of thymus function in DBA/2 mice (Hsu et al., 2003). Third, in thymi enlarged after castration, we found a threefold reduction in Tbata expression in TECs from 4-mo-old mice 1 wk after surgery compared with sham castrated mice. In this same time frame, TEC proliferation increases and a 2.5-fold increase in TEC numbers is observed (Gray et al., 2006; Williams et al., 2008). These findings suggest that Tbata-mediated cell cycle arrest is reversible in TECs, as we observed in our in vitro experiments. Fourth, we observed a 5–10-fold increase in Tbata expression in mature mTECs (UEA$^+$MHC class II$^{hi}$) compared with the preceding stage (UEA$^+$ MHC Class II$^{lo}$) of mTEC development. Mature mTECs cease proliferation during this developmental transition. We also observed increased proliferation of mature mTECs in *Tbata*$^{-/-}$ mice, suggesting that Tbata may also play a role in promoting exit from the cell cycle during mTEC development. Together, these data suggest that Tbata is involved in the negative regulation of TEC proliferation.

To further explore how Tbata might regulate TEC proliferation, we characterized the function of the Tbata protein. We showed that Tbata mediates a profound growth arrest in cells by specifically interacting with Uba3. This interaction inhibits the Nedd8 pathway and results in cell cycle arrest, because neddylation of cullins is a prerequisite for targeted degradation of several cell cycle control proteins (Podust et al., 2000; Doronkin et al., 2003). Linkage of Tbata to the Nedd8 pathway was confirmed by showing that Tbata-mediated growth arrest was attenuated by overexpression of Uba3, whereas overexpression of an Uba3 mutant that does not bind Tbata did not affect Tbata-mediated growth arrest. Based on our experimental evidence, it appears that KIF17 does not affect Tbata-mediated growth suppression. Therefore, Tbata exerts a negative regulation on cell cycle progression that is consistent with blocking the Nedd8 pathway. These data support Tbata as a negative regulator of TEC proliferation and provide a molecular mechanism for its effect.

Different steps of the Nedd8 pathway have been used in cells to provide additional levels of cell cycle regulation. Mechanisms are based on selective de-neddylation of cullins by the COP9 signalsome protein complex or other proteins (Gong et al., 2000; Yang et al., 2002; Gan-Erdene et al., 2003; Mendoza et al., 2003; von Arnim, 2003; Wu et al., 2003). NUB1 sequesters and degrades Nedd8 monomers and Nedd8 conjugates (Kamitani et al., 2001; Kito et al., 2001) and TIP120A binds to cullins blocking their modification by Nedd8 (Yogosawa et al., 1999; Hwang et al., 2003). Our data reveal that Tbata mediates a novel inhibition mechanism of the proximal Nedd8 pathway by preventing formation of the Nedd8 E1 via its disruption of the Uba3–AppBp1 complex. The crystal structure of the human Uba3–AppBp1 heterodimer suggests how Tbata might disrupt this complex (Walden et al., 2003). 72 aa of Uba3 contact AppBp1 to form functional adenylation and catalytic cysteine domains. An interface between Uba3 and AppBp1 is mediated by a closely spaced high-affinity interaction of 32 residues of Uba3 within aa 270–334 that directly contact AppBp1. Tbata specifically interacts with a portion of Uba3 that includes aa 214–321, a region that contains 28 residues that contact AppBp1 (Walden et al., 2003). Because of the close proximity of AppBp1 to Uba3 at aa 214–321, it is likely that a high-affinity Tbata interaction with Uba3 in this region would sterically inhibit the binding of AppBp1 to Uba3 and block Nedd8 E1 formation. Therefore, the restricted expression of Tbata in thymus appears to mediate a unique cell cycle control mechanism in TECs to regulate thymus function.

The dominant phenotypic feature of Tbata deficiency is the improved thymus function observed in aged *Tbata*$^{-/-}$ mice compared with WT mice. One likely explanation for the *Tbata*$^{-/-}$ phenotype is that enhanced proliferation of thymic stromal cells in aged mice creates a larger niche size that can accommodate more thymocytes. This change results in greater thymus function in aged mice compared with the WT control, but does not affect T cell development or thymus architecture. Although thymus function decreases during aging in *Tbata*$^{-/-}$ mice, it occurs at a slower rate. In 6–9-mo-old *Tbata*$^{-/-}$ mice, we observed statistically significant increases in total TEC number and in the number of proliferating UEA$^+$ cells. The phenotype of *Tbata*$^{-/-}$ mice appears to depend on changes in thymic stromal cells because Tbata is only expressed in these cells (Flomerfelt et al., 2000) and *Tbata*$^{-/-}$ *Rag2*$^{-/-}$ mice show a robust and more rapid thymic reconstitution compared with *Rag2*$^{-/-}$ littermates after BMT from WT donor mice, thereby mapping the function to the TEC compartment. Rapid reconstitution in the *Tbata*$^{-/-}$*Rag2*$^{-/-}$ may be caused by enhanced stromal cell proliferation and a more rapid response to increase niche size when normal thymocytes

enter the thymus. A similar model has been proposed to explain the more rapid reconstitution of IL-7R$^{-/-}$ mice compared with *Rag2*$^{-/-}$ mice (Prockop and Petrie, 2004). It is probable that thymus function depends on integration between niche size and precursor import. For example, studies using IGF-1 to enhance thymus function concluded that all parameters of thymus function, including import, appear to be related to available niche size (Chu et al., 2008). In the case of the *Tbata*$^{-/-}$*Rag2*$^{-/-}$, it is possible that the "reception" for recently imported precursor cells favors rapid expansion and onset of differentiation.

The regulation of thymic stromal cell proliferation is likely involved in controlling thymus function in response to environmental signals, aging, or disease states. We hypothesize that Tbata regulates thymus function by a reversible negative regulation of stromal cell proliferation and propose that this creates a greater availability of thymus stromal cell niches accessible for thymocyte development. It is possible that the Tbata–Uba3 interaction will provide a molecular target for developing therapeutic tools to enhance T cell production in adult immunocompromised patients and to augment function of the thymus in aged patients.

## MATERIALS AND METHODS

**Plasmids, cell lines, mice, and reagents.** Tbata transcript variant 3 (AF257502; available from GenBank/EMBL/DDBJ under accession no. NM_023064), and Tbata transcript variant 5 (AF257503; available from GenBank/EMBL/DDBJ under accssion no. NM_001017407) cDNAs were cloned from mouse thymus (Flomerfelt et al., 2000). Human AppBp1 (BC000480) and mouse Uba3 (BC002002) cDNAs were obtained from the IMAGE consortium. Human Uba3 cDNA was a gift from E. Yeh (University of Texas M.D. Anderson Cancer Center, Houston, TX). GST-Jun plasmid was a gift from Z.-G. Liu (National Cancer Institute, Bethesda, MD). Mouse KIF17 fused to mCherry was purchased from GeneCopoeia Inc. C57BL/6, DBA/2, and Ly5.1 congenic mice were obtained from the National Cancer Insitute (NCI), Frederick, animal facility. C57BL/6 *Rag2*$^{-/-}$ mice were obtained from Taconic. *Tbata*$^{-/-}$*Rag2*$^{-/-}$ or *Rag2*$^{-/-}$ littermates were bred in our mouse facility. All animal care, handling, and procedures were done following protocols detailed in Animal Science Protocols approved by the NCI Animal Care and Use Committee using guidelines approved by the National Institutes of Health Animal Research Advisory Committee.

**KO construction.** A P1 clone was used to construct a targeting vector with a 2.3-kb EcoRV-Xma1 fragment upstream of the thymus-specific start site and a 4.5-kb Xho1–BamH1 fragment downstream of the termination codon (Flomerfelt et al., 2000). The linearized targeting vector was transfected into E14.1 ES cells derived from 129 mice. Homologous recombination was confirmed by Southern blot analysis (Fig. S2, A–D). Chimeric mice were bred to C57BL/6 mice. Heterozygous mice were backcrossed onto a C57BL/6 background four times, and heterozygotes were interbred to obtain *Tbata*$^{-/-}$ mice and control WT littermates.

**FACS analysis.** FACS data were collected on a FACSCalibur or a LSRII (both from BD) and analyzed using CellQuest (BD) and FlowJo (Tree Star, Inc.) software. 10 µg/ml 2.4G2 was added to $10^7$ cells/ml. Double-negative subsets were studied on gated lineage-negative cells using anti–CD44-PE and anti–CD25-FITC along with biotinylated or Tricolor-conjugated anti-lineage markers (CD3, CD4, CD8, CD11b, Pan NK, B220, and Ter119), followed by Streptavidin Tricolor or Streptavidin allophycocyanin conjugates. TEC analysis was done on CD45- or CD90-negative cells and included HSA$^-$ cells to quantitate TEC numbers in the aging studies. Ki67 staining was done on fixed cells using the BrdU staining kit (BD) after surface staining with UEA-FITC, Ly51-PE, Class II-Bio-Pacific blue avidin, and CD45 PE Cy5.5. Cells stained with Ki67 were not DNase-treated.

**TEC isolation.** The thymus was dissected and minced with a Mickle Tissue Homogenizer. The tissue was resuspended in RPMI, and 50 µl of Liberase4 (28 U/ml) and DNase1 (2 mg/ml) were added and incubated for 15 min at 37°C, shaking at 250 RPM. For sorting and proliferation analysis, the cell suspension was thymocyte-depleted using the anti-CD90 MACS system (Miltenyi Biotec).

**Immunohistochemistry.** Frozen thymus sections were incubated in 1% 24g2, 3% normal donkey serum. Keratin staining was done with rat anti-Keratin 5 (2 µg/section; Covance) and rabbit anti-Keratin 8 (2 µg/section; Troma-1; Developmental Studies Hybridoma Bank, The University of Iowa) and visualized with the appropriate FITC- or Texas red–conjugated secondary antibodies. Images were collected on an Olympus IX71 with an UPanFLN20x/0.5 objective using an iCys Research Laser Scanning Cytometer. A series of overlapping 200× magnification images of the whole section were obtained and digitally stitched together using an iCys Research Imaging Cytometer and iCyte Cytometric Analysis Software 3.2. The software produces the horizontal lines when the image is digitally stitched together.

**Relative quantitation of Tbata isoforms.** RNA from sorted stromal cells was linearly amplified using the RiboAmp HS Plus (Applied Biosystems) kit. cDNA synthesis was performed using random primers and 3–5 µg of total RNA. Real-time PCR quantitation was performed using the LightCycler (Roche). Standard curves for quantitation were generated from serial dilutions of cDNA from 5 µg of total thymus mRNA from C57BL/6 mice. Undiluted cDNA was assigned an arbitrary value, and the instrument software calculated concentration values. Assays were designed to amplify all Tbata isoforms or only the Ttv3 or Ttv5 isoforms. Primer sequences are available upon request. For the aging studies on sorted TEC, the relative expression was normalized to input RNA. For all other experiments, Tbata levels were normalized using GAPDH expression in the same samples. All experiments were done in triplicate and were repeated 3–5 times with independent samples.

**GST pulldown assays.** Recombinant GST, GST-Tbata, and GST-Jun fusion protein lysates were purified from bacteria. Radiolabeled proteins were produced using separate coupled transcription-translation reactions (Promega). A sample of the reaction was run on a gel to confirm that equal amounts of radiolabeled proteins were mixed with equal amounts of either GST or GST fusion proteins bound to glutathione-coated Sepharose beads. Samples were incubated for 2–12 h at 4°C, followed by five 1-ml washes using ice-cold TBS with 0.1% Tween-20. Bound proteins were eluted from the beads in PAGE sample buffer at 70°C, and subjected to PAGE.

**Yeast two-hybrid analysis.** The Matchmaker Yeast Two-Hybrid System 3 (Takara Bio Inc.) was used following the manufacturer's recommendations to identify proteins that interact with Tbata. A full-length cDNA of the Ttv3 Tbata isoform was fused to the Gal4 DNA binding domain in the vector pGBKT7. This construct did not activate reporter genes based on growth analysis and was used as the bait. Prey constructs were obtained from a day 18 mouse embryo library cloned into the vector pACT2. The day 18 embryo has a fully functional thymus that expresses Tbata (Flomerfelt et al., 2000).

**DiI generational analysis.** 24 h after transfection, cells were labeled with DiI. 1 h later, DiI label intensity was analyzed by FACS (day 0) and each day after transfection. We noted a slight increase in DiI intensity in nondividing cells over a 4-d period. MODFIT software (Verity Software House) was used to analyze the FACS data using a progressive Gaussian estimation based on the intensity and the SD of the parent population. Profiles were generated to measure cell division by gating the analysis on EGFP$^+$, Ttv3-EGFP$^+$, or EGFP$^-$ cells.

**Statistical analysis.** Statistical analysis was performed using StatView 5.0.1 or Microsoft Excel software. Error bars on graphs show the SD.

Where indicated, studies were analyzed using Student's *t* test, with a value of 0.05 or less considered significant.

**Online supplemental material.** Fig. S1 shows Tbata expression in the cerebellum and testes, sort scheme for TEC cells, KIF17 expression analysis in different tissues and cells, and the effect of KIF17 on Tbata-mediated growth suppression. Fig. S2 shows the generation and verification of the *Tbata*$^{-/-}$, and stained sections of WT and *Tbata*$^{-/-}$ brains and testes. Fig. S3 shows keratin5 and keratin8 staining of WT and *Tbata*$^{-/-}$ thymus and the T cell response to DNP-OVA of WT and *Tbata*$^{-/-}$ mice. Fig. S4 shows enumeration of splenic B cells 3 wk after BM transplantation in *Rag2*$^{-/-}$ and *Tbata*$^{-/-}$ mice. Online supplemental material is available at http://www.jem.org/cgi/content/full/jem.20092759/DC1.

The authors thank Krishnendu Roy, Allan Weissman, Emanuela Lacana, Yu-Waye Chu, Richard Hodes, Kirsten Williams, and Fran Hakim, for helpful discussions about the manuscript. Vanessa Baxendale kindly provided her expertise in evaluating testis anatomy. The National Institute of Allergy and Infectious Disease Gene Targeting Unit produced the *Tbata*$^{-/-}$.

The authors have no commercial affiliations or competing financial interests to disclose.

**Submitted: 24 December 2009**
**Accepted: 7 September 2010**

## REFERENCES

Anderson, G., and E.J. Jenkinson. 2001. Lymphostromal interactions in thymic development and function. *Nat. Rev. Immunol.* 1:31–40. doi:10.1038/35095500

Anderson, G., B.C. Harman, K.J. Hare, and E.J. Jenkinson. 2000. Microenvironmental regulation of T cell development in the thymus. *Semin. Immunol.* 12:457–464. doi:10.1006/smim.2000.0260

Bloom, J., V. Amador, F. Bartolini, G. DeMartino, and M. Pagano. 2003. Proteasome-mediated degradation of p21 via N-terminal ubiquitinylation. *Cell.* 115:71–82. doi:10.1016/S0092-8674(03)00755-4

Chu, Y.W., S. Schmitz, B. Choudhury, W. Telford, V. Kapoor, S. Garfield, D. Howe, and R.E. Gress. 2008. Exogenous insulin-like growth factor 1 enhances thymopoiesis predominantly through thymic epithelial cell expansion. *Blood.* 112:2836–2846.

Doronkin, S., I. Djagaeva, and S.K. Beckendorf. 2003. The COP9 signalosome promotes degradation of Cyclin E during early Drosophila oogenesis. *Dev. Cell.* 4:699–710. doi:10.1016/S1534-5807(03)00121-7

Flomerfelt, F.A., M.G. Kim, and R.H. Schwartz. 2000. Spatial, a gene expressed in thymic stromal cells, depends on three-dimensional thymus organization for its expression. *Genes Immun.* 1:391–401. doi:10.1038/sj.gene.6363695

Gan-Erdene, T., K. Nagamalleswari, L. Yin, K. Wu, Z.Q. Pan, and K.D. Wilkinson. 2003. Identification and characterization of DEN1, a deneddylase of the ULP family. *J. Biol. Chem.* 278:28892–28900. doi:10.1074/jbc.M302890200

Gong, L., and E.T. Yeh. 1999. Identification of the activating and conjugating enzymes of the NEDD8 conjugation pathway. *J. Biol. Chem.* 274:12036–12042. doi:10.1074/jbc.274.17.12036

Gong, L., T. Kamitani, S. Millas, and E.T. Yeh. 2000. Identification of a novel isopeptidase with dual specificity for ubiquitin- and NEDD8-conjugated proteins. *J. Biol. Chem.* 275:14212–14216. doi:10.1074/jbc.275.19.14212

Gray, D.H., N. Seach, T. Ueno, M.K. Milton, A. Liston, A.M. Lew, C.C. Goodnow, and R.L. Boyd. 2006. Developmental kinetics, turnover, and stimulatory capacity of thymic epithelial cells. *Blood.* 108:3777–3785. doi:10.1182/blood-2006-02-004531

Gray, D., J. Abramson, C. Benoist, and D. Mathis. 2007. Proliferative arrest and rapid turnover of thymic epithelial cells expressing Aire. *J. Exp. Med.* 204:2521–2528. doi:10.1084/jem.20070795

Hatten, M.E., and N. Heintz. 1995. Mechanisms of neural patterning and specification in the developing cerebellum. *Annu. Rev. Neurosci.* 18:385–408.

Hirokawa, N., and R. Takemura. 2004. Kinesin superfamily proteins and their various functions and dynamics. *Exp. Cell Res.* 301:50–59. doi:10.1016/j.yexcr.2004.08.010

Hori, T., F. Osaka, T. Chiba, C. Miyamoto, K. Okabayashi, N. Shimbara, S. Kato, and K. Tanaka. 1999. Covalent modification of all members of human cullin family proteins by NEDD8. *Oncogene.* 18:6829–6834. doi:10.1038/sj.onc.1203093

Hsu, H.C., H.G. Zhang, L. Li, N. Yi, P.A. Yang, Q. Wu, J. Zhou, S. Sun, X. Xu, X. Yang, et al. 2003. Age-related thymic involution in C57BL/6J x DBA/2J recombinant-inbred mice maps to mouse chromosomes 9 and 10. *Genes Immun.* 4:402–410. doi:10.1038/sj.gene.6363982

Hsu, H.C., L. Li, H.G. Zhang, and J.D. Mountz. 2005. Genetic regulation of thymic involution. *Mech. Ageing Dev.* 126:87–97. doi:10.1016/j.mad.2004.09.016

Huang, S., P. Law, K. Francis, B.O. Palsson, and A.D. Ho. 1999. Symmetry of initial cell divisions among primitive hematopoietic progenitors is independent of ontogenic age and regulatory molecules. *Blood.* 94:2595–2604.

Hwang, J.W., K.W. Min, T.A. Tamura, and J.B. Yoon. 2003. TIP120A associates with unneddylated cullin 1 and regulates its neddylation. *FEBS Lett.* 541:102–108. doi:10.1016/S0014-5793(03)00321-1

Irla, M., D. Puthier, R. Le Goffic, G. Victorero, T. Freeman, P. Naquet, M. Samson, and C. Nguyen. 2003. Spatial, a new nuclear factor tightly regulated during mouse spermatogenesis. *Gene Expr. Patterns.* 3:135–138. doi:10.1016/S1567-133X(03)00024-3

Irla, M., M. Saade, C. Fernandez, L. Chasson, G. Victorero, N. Dahmane, G. Chazal, and C. Nguyen. 2007. Neuronal distribution of spatial in the developing cerebellum and hippocampus and its somatodendritic association with the kinesin motor KIF17. *Exp. Cell Res.* 313:4107–4119. doi:10.1016/j.yexcr.2007.09.006

Jenkinson, W.E., A. Bacon, A.J. White, G. Anderson, and E.J. Jenkinson. 2008. An epithelial progenitor pool regulates thymus growth. *J. Immunol.* 181:6101–6108.

Kamitani, T., K. Kito, T. Fukuda-Kamitani, and E.T. Yeh. 2001. Targeting of NEDD8 and its conjugates for proteasomal degradation by NUB1. *J. Biol. Chem.* 276:46655–46660. doi:10.1074/jbc.M108636200

Kim, M.G., C. Chen, F.A. Flomerfelt, R.N. Germain, and R.H. Schwartz. 1998. A subtractive PCR-based cDNA library made from fetal thymic stromal cells. *J. Immunol. Methods.* 213:169–182. doi:10.1016/S0022-1759(98)00031-3

Kito, K., E.T. Yeh, and T. Kamitani. 2001. NUB1, a NEDD8-interacting protein, is induced by interferon and down-regulates the NEDD8 expression. *J. Biol. Chem.* 276:20603–20609. doi:10.1074/jbc.M100920200

Klug, D.B., E. Crouch, C. Carter, L. Coghlan, C.J. Conti, and E.R. Richie. 2000. Transgenic expression of cyclin D1 in thymic epithelial precursors promotes epithelial and T cell development. *J. Immunol.* 164:1881–1888.

Mendoza, H.M., L.N. Shen, C. Botting, A. Lewis, J. Chen, B. Ink, and R.T. Hay. 2003. NEDP1, a highly conserved cysteine protease that deNEDDylates Cullins. *J. Biol. Chem.* 278:25637–25643. doi:10.1074/jbc.M212948200

Morimoto, M., T. Nishida, R. Honda, and H. Yasuda. 2000. Modification of cullin-1 by ubiquitin-like protein Nedd8 enhances the activity of SCF(skp2) toward p27(kip1). *Biochem. Biophys. Res. Commun.* 270:1093–1096. doi:10.1006/bbrc.2000.2576

Morimoto, M., T. Nishida, Y. Nagayama, and H. Yasuda. 2003. Nedd8-modification of Cul1 is promoted by Roc1 as a Nedd8-E3 ligase and regulates its stability. *Biochem. Biophys. Res. Commun.* 301:392–398. doi:10.1016/S0006-291X(02)03051-6

O'Hagan, R.C., M. Ohh, G. David, I.M. de Alboran, F.W. Alt, W.G. Kaelin Jr., and R.A. DePinho. 2000. Myc-enhanced expression of Cul1 promotes ubiquitin-dependent proteolysis and cell cycle progression. *Genes Dev.* 14:2185–2191. doi:10.1101/gad.827200

Ohh, M., W.Y. Kim, J.J. Moslehi, Y. Chen, V. Chau, M.A. Read, and W.G. Kaelin Jr. 2002. An intact NEDD8 pathway is required for Cullin-dependent ubiquitylation in mammalian cells. *EMBO Rep.* 3:177–182. doi:10.1093/embo-reports/kvf028

Podust, V.N., J.E. Brownell, T.B. Gladysheva, R.S. Luo, C. Wang, M.B. Coggins, J.W. Pierce, E.S. Lightcap, and V. Chau. 2000. A Nedd8 conjugation pathway is essential for proteolytic targeting of

p27Kip1 by ubiquitination. *Proc. Natl. Acad. Sci. USA*. 97:4579–4584. doi:10.1073/pnas.090465597

Prockop, S.E., and H.T. Petrie. 2004. Regulation of thymus size by competition for stromal niches among early T cell progenitors. *J. Immunol.* 173:1604–1611.

Rabut, G., and M. Peter. 2008. Function and regulation of protein neddylation. 'Protein modifications: beyond the usual suspects' review series. *EMBO Rep.* 9:969–976. doi:10.1038/embor.2008.183

Robles, A.I., F. Larcher, R.B. Whalin, R. Murillas, E. Richie, I.B. Gimenez-Conti, J.L. Jorcano, and C.J. Conti. 1996. Expression of cyclin D1 in epithelial tissues of transgenic mice results in epidermal hyperproliferation and severe thymic hyperplasia. *Proc. Natl. Acad. Sci. USA*. 93:7634–7638. doi:10.1073/pnas.93.15.7634

Saade, M., M. Irla, J. Govin, G. Victorero, M. Samson, and C. Nguyen. 2007. Dynamic distribution of Spatial during mouse spermatogenesis and its interaction with the kinesin KIF17b. *Exp. Cell Res.* 313:614–626. doi:10.1016/j.yexcr.2006.11.011

Shinkai, Y., G. Rathbun, K.P. Lam, E.M. Oltz, V. Stewart, M. Mendelsohn, J. Charron, M. Datta, F. Young, A.M. Stall, et al. 1992. RAG-2-deficient mice lack mature lymphocytes owing to inability to initiate V(D)J rearrangement. *Cell*. 68:855–867. doi:10.1016/0092-8674(92)90029-C

Singer, J.D., M. Gurian-West, B. Clurman, and J.M. Roberts. 1999. Cullin-3 targets cyclin E for ubiquitination and controls S phase in mammalian cells. *Genes Dev.* 13:2375–2387. doi:10.1101/gad.13.18.2375

Tateishi, K., M. Omata, K. Tanaka, and T. Chiba. 2001. The NEDD8 system is essential for cell cycle progression and morphogenetic pathway in mice. *J. Cell Biol.* 155:571–579. doi:10.1083/jcb.200104035

von Arnim, A.G. 2003. On again-off again: COP9 signalosome turns the key on protein degradation. *Curr. Opin. Plant Biol.* 6:520–529. doi:10.1016/j.pbi.2003.09.006

Wada, H., E.T. Yeh, and T. Kamitani. 2000. A dominant-negative UBC12 mutant sequesters NEDD8 and inhibits NEDD8 conjugation in vivo. *J. Biol. Chem.* 275:17008–17015. doi:10.1074/jbc.275.22.17008

Walden, H., M.S. Podgorski, and B.A. Schulman. 2003. Insights into the ubiquitin transfer cascade from the structure of the activating enzyme for NEDD8. *Nature*. 422:330–334. doi:10.1038/nature01456

Williams, K.M., P.J. Lucas, C.V. Bare, J. Wang, Y.W. Chu, E. Tayler, V. Kapoor, and R.E. Gress. 2008. CCL25 increases thymopoiesis after androgen withdrawal. *Blood*. 112:3255–3263. doi:10.1182/blood-2008-04-153627

Wu, K., K. Yamoah, G. Dolios, T. Gan-Erdene, P. Tan, A. Chen, C.G. Lee, N. Wei, K.D. Wilkinson, R. Wang, and Z.Q. Pan. 2003. DEN1 is a dual function protease capable of processing the C terminus of Nedd8 and deconjugating hyper-neddylated CUL1. *J. Biol. Chem.* 278:28882–28891. doi:10.1074/jbc.M302888200

Xirodimas, D.P., M.K. Saville, J.C. Bourdon, R.T. Hay, and D.P. Lane. 2004. Mdm2-mediated NEDD8 conjugation of p53 inhibits its transcriptional activity. *Cell*. 118:83–97. doi:10.1016/j.cell.2004.06.016

Yang, X., S. Menon, K. Lykke-Andersen, T. Tsuge, Di Xiao, X. Wang, R.J. Rodriguez-Suarez, H. Zhang, and N. Wei. 2002. The COP9 signalosome inhibits p27(kip1) degradation and impedes G1-S phase progression via deneddylation of SCF Cul1. *Curr. Biol.* 12:667–672. doi:10.1016/S0960-9822(02)00791-1

Yeh, E.T., L. Gong, and T. Kamitani. 2000. Ubiquitin-like proteins: new wines in new bottles. *Gene*. 248:1–14. doi:10.1016/S0378-1119(00)00139-6

Yogosawa, S., K. Kayukawa, T. Kawata, Y. Makino, S. Inoue, A. Okuda, M. Muramatsu, and T. Tamura. 1999. Induced expression, localization, and chromosome mapping of a gene for the TBP-interacting protein 120A. *Biochem. Biophys. Res. Commun.* 266:123–128. doi:10.1006/bbrc.1999.1773

## SUPPLEMENTAL MATERIAL

**Flomerfelt et al., http://www.jem.org/cgi/content/full/jem.20092759/DC1**

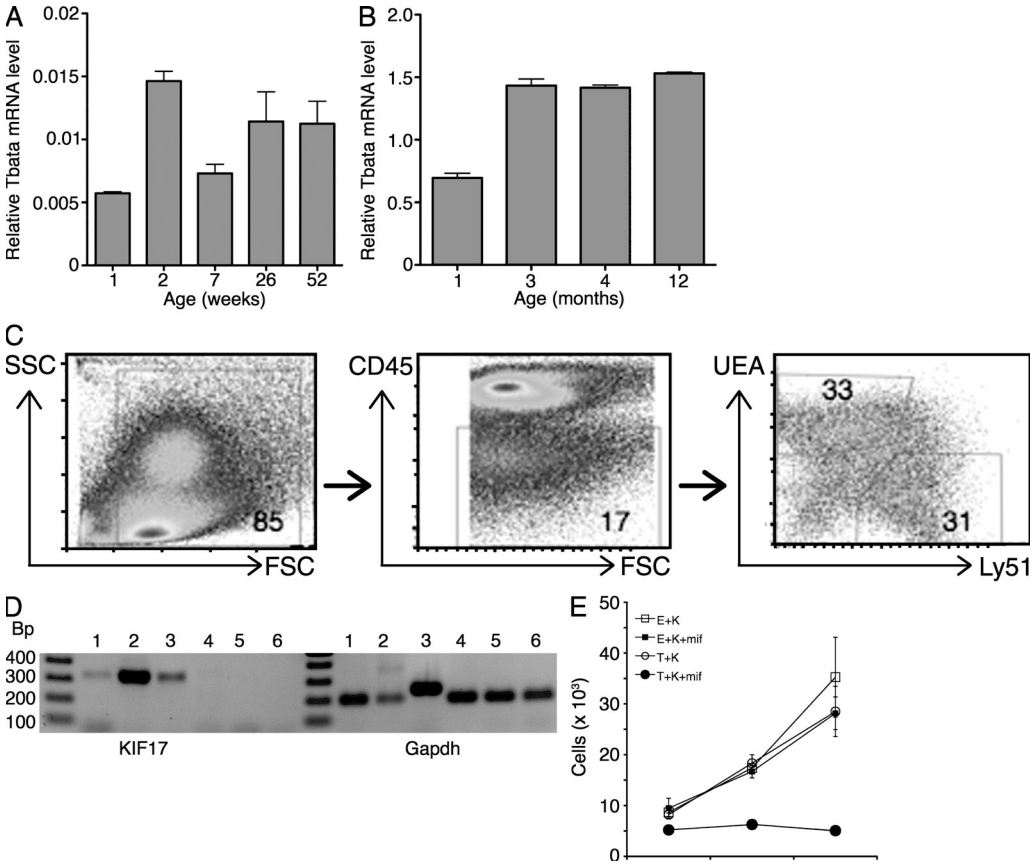


**Figure S1. Analysis of Tbata and KIF17 expression and the effect of KIF17 on Tbata-mediated growth suppression.** (A) Real-time PCR analysis of Tbata expression in the cerebellum during aging in C57BL/6 mice. Two to three mice were used for each time point, and the PCR analysis was repeated at least nine times. Error bars denote the SD. (B) Real-time PCR analysis of Tbata expression in the testes during aging in C57BL/6 mice. Two to three mice were used for each time point, and the PCR analysis was repeated at least nine times. Error bars denote the SD. (C) Scheme used to sort UEA$^+$ and Ly51$^+$ stromal cells from 1- and 10-mo-old mice. Stromal cells were prepared and stained as described in the Materials and methods and sorted on a FACSVantage SE. Both UEA$^+$ and Ly51$^+$ cells (right) were sorted from live-gated (left) CD45$^-$ gated (middle) cells. Sorted cells were analyzed by FACS and were of 90% or greater purity. (D) RT-PCR analysis of KIF17 and GAPDH expression in the following areas: 1, brain; 2, testes; 3, HEK 293 cells; 4, thymus; 5, purified TEC; and 6, NIH3T3 cells. The experiment was repeated three times using RNA from different sources with the same results. (E) KIF17 does not affect Tbata-dependent growth suppression. EGFP-C or Ttv3-C cells were transfected with a KIF17-mCherry fusion protein expression plasmid, and mifepristone was added to induce EGFP or Ttv3-EGFP expression. Cells expressing KIF17-mCherry (+K) in the presence (+mif samples) or absence of Ttv3-EGFP (T) or EGFP (E) were counted over a 3-d period. The data shown is representative of three experiments done in triplicate. Error bars denote the SD.

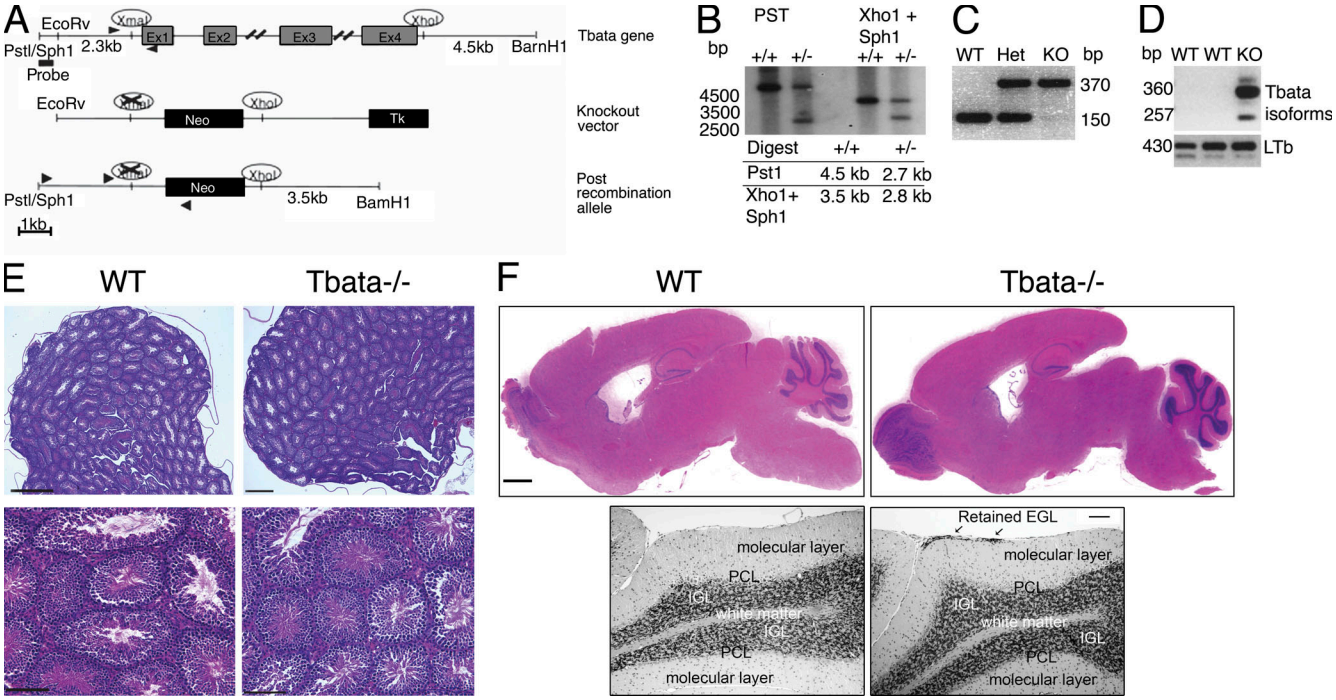


**Figure S2. Generation of the *Tbata* KO.** (A) Genomic structure of *Tbata*, targeting construct, and genomic structure after homologous recombination are shown. Black arrowheads show relative position of primers used to identify homologous recombinants and to genotype mice. (B) Southern blots of Pst1- or Xho1- and Sph1-digested genomic DNA obtained from ES cells verify homologous recombination. Bands corresponding to the disrupted allele are marked with an asterisk, and the expected sizes are shown below the blot. (C) Genomic PCR was used to type mice bearing heterozygote (Het), *Tbata*$^{-/-}$ (KO), and WT alleles. (D) RT-PCR was used to analyze Tbata mRNA expression in WT and *Tbata*$^{-/-}$ mice. A primer set was also used to amplify lymphotoxin-β (LTb) as a positive control. Similar results were obtained for 10 different WT or *Tbata*$^{-/-}$ mice. (E) Hematoxylin and eosin (H&E) stain of *Tbata*$^{-/-}$ and WT testes. (top) A low magnification image (bar, 0.5 mm) image. (bottom) 200× magnification of the late stages of tubule development (bar, 0.1 mm). The images are representative of that observed in six stained sections from four to five WT and *Tbata*$^{-/-}$ mice. (F) H&E stained sections of brain from WT or *Tbata*$^{-/-}$ mice. (top) A low power image (bar, 1 mm) image of the whole brain. (bottom) A 100× magnification of the cerebellum showing 5-ethynyl-2-deoxyuridine labeling detailing a retained nest of EGL in an adult mouse (bar, 100 µm). The images are representative of that observed in 16 sections/brain from 5 WT and 5 *Tbata*$^{-/-}$ mice.

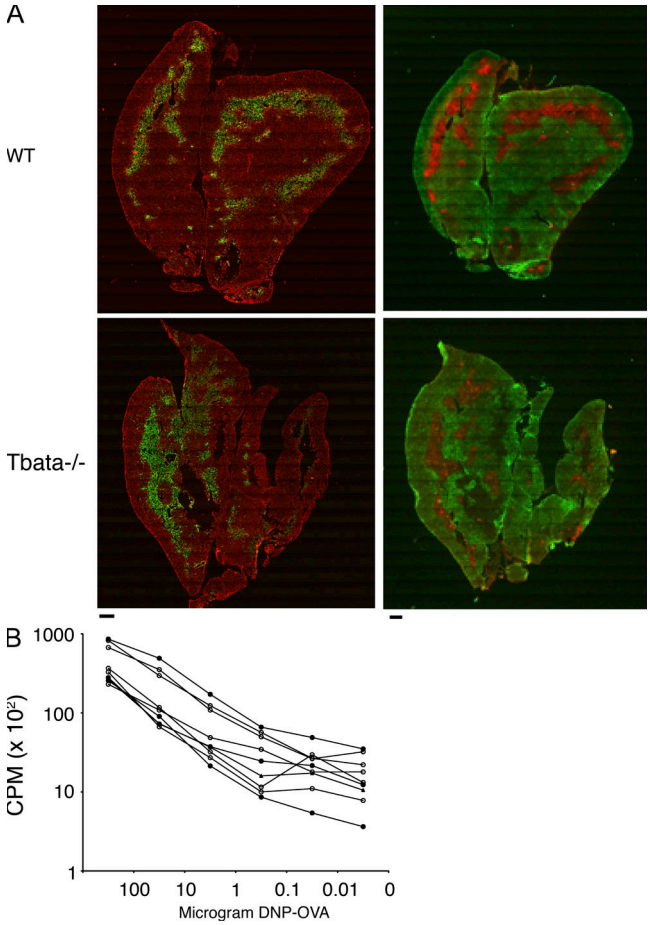


**Figure S3. Thymus organization and T cell response are normal in *Tbata*$^{-/-}$ mice.** (B) Frozen thymus sections of similar size from 5-mo-old WT or *Tbata*$^{-/-}$ mice were stained with K5 (green) and K8 (red) or with Ly51 (green) and UEA (red) to stain cTEC or mTEC and to observe overall thymus organization. No gross anatomical defects were found in the *Tbata*$^{-/-}$ thymus. The entire thymus sections from WT mice are shown on the top, and the entire *Tbata*$^{-/-}$ sections are on the bottom. Sections stained with species-matched purified IgG as primary antibody lacked any staining pattern (n). Bars, 400 µm. Similar results were obtained in five to six independent experiments using different mice. (B) Proliferation data assessed by [$^3$H]thymidine uptake for purified 4 × 10$^5$ CD4 T cells from mice immunized with $DNP_6$-OVA that were cultured with 1 × 10$^5$ irradiated APC and varying amounts of $DNP_6$-OVA for 72 h. Tritiated thymidine was added during the last 18 h of the culture. CD4 T cells were obtained from WT (●, *n* = 3) or *Tbata*$^{-/-}$ (○, *n* = 5) mice.

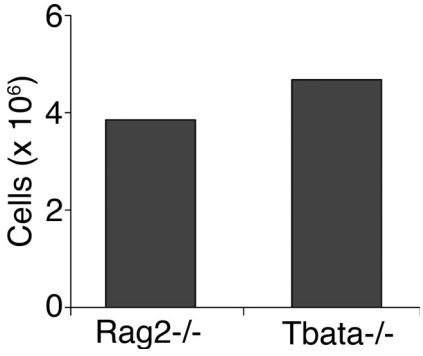


**Figure S4. Similar numbers of donor splenic B cells (Ly5.1$^+$, B220$^+$) were analyzed 3 wk after BMT to confirm successful BM transplant.** FACS data obtained from a single mouse representative of the results obtained from seven *Tbata*$^{-/-}$*Rag2*$^{-/-}$ and six *Rag2*$^{-/-}$ mice.